INVESTIGATION OF THE PROCESSING PARAMETERS OF A 3D WOVEN REINFORCEMENT

Andreas Endruweit, Dhiren K. Modi and Andrew C. Long

School of Mechanical, Materials and Manufacturing Engineering, University of Nottingham,
University Park, Nottingham, NG7 2RD, U.K.
dhiren.modi@nottingham.ac.uk

ABSTRACT

For a carbon fibre 3D reinforcement with through-thickness angle interlock weave architecture, the compressibility is relatively high because of the large amount of void space. in cyclic compression, the compressibility is reduced after the first cycle and remains approximately constant in the subsequent cycles. Microscopic study of the fabric structure suggests that permanent reordering of the fibre bundles during the first load cycle implies moving of binder tows into the inter-bundle voids, locally bending the weft bundles and pushing the warp bundles apart. While, at low levels of fabric compression, the layer height is reduced mainly by local reduction of the height of voids, at higher compression levels, it is reduced by bundle compression and change of the bundle cross-section. The significant reduction of the inter-bundle void volume in compression is correlated to the decrease in permeability with increasing fibre volume fraction. The fabric permeability is determined by the configuration of the binder tows: The angle between the fabric weft direction and the pattern of the binder tows is reflected in the orientation of the principal permeability axes. The through-thickness permeability is dominated by flow-enhancing through-thickness channels in the fabric structure, formed around the binder tows.

1. INTRODUCTION

Reinforcements for polymer composites are typically based on glass, aramid or carbon fibres, with various modifications of each type, which depend on the microscopic material structure. Mainly to improve the handling of the dry reinforcement, fabrics with a variety of geometrical structures (architectures) are produced from the fibres, using textile processes such as weaving, knitting and braiding. Each fabric architecture has specific fields of application, mainly depending on the geometry of the component to be produced and the loads it is supposed to bear. The vast majority of textile reinforcements show two-dimensional (2D) architectures, which generally allow good tensile and flexural properties to be obtained, but are less favourable regarding fatigue and delamination. To overcome these limitations and to allow net-shape preform manufacture, in particular for manufacture of thick components, three-dimensional (3D) fabric architectures, produced by 3D weaving processes, have been developed more recently. These consist frequently of layers of aligned non-crimp fibres, which generally show better mechanical properties than the crimped fibres found in most 2D reinforcements, e.g. 2D woven fabrics. Additional binder fibres, which follow paths through the fabric thickness, hold the layers together and provide toughness and resistance to delamination.

The fabric processing parameters relate to the various steps in composites manufacture, in particular forming and impregnation with a liquid matrix system, and significantly affect the properties of the finished component. They include drape, compression behaviour and permeability. For 3D fabrics, these parameters have been individually investigated by Potluri et al. [1], Desplentere et al. [2] and Adanur et al. [3]. However, a systematic approach to investigate these parameters and the correlations between them for a specific reinforcement has not been reported so far. This study deals with the experimental characterisation of the processing parameters, in particular

compressibility and permeability, for an example of 3D reinforcements, relates them to the textile architecture and compares them quantitatively with the properties of examples for commercial 2D reinforcements.

2. MATERIAL

The processing parameters were studied for the example of a carbon fibre 3D reinforcement with through-thickness angle interlock weave architecture. The fabric comprises of two layers of 12K tows in the warp direction, three layers of 6K tows in the weft direction and 3K binder tows, alternating with the 12K tows in the warp direction. For illustration, an idealised model of the unit cell of the architecture, generated using the TexGen geometry pre-processor [4], is depicted in Figure 1. The dry thickness of the uncompressed fabric, measured using a Vernier calliper at minimal applied pressure, is typically 2.2 mm, and the superficial density was found to be S = (1.438 ± 0.021) kg/m^2.

If applicable, the processing parameters determined for the 3D reinforcement are compared to the corresponding parameters of conventional 2D carbon fibre fabrics, a 5-harness satin weave fabric with a superficial density S = 302 g/m^2 and a UD fabric with a superficial density S = 342 g/m^2.

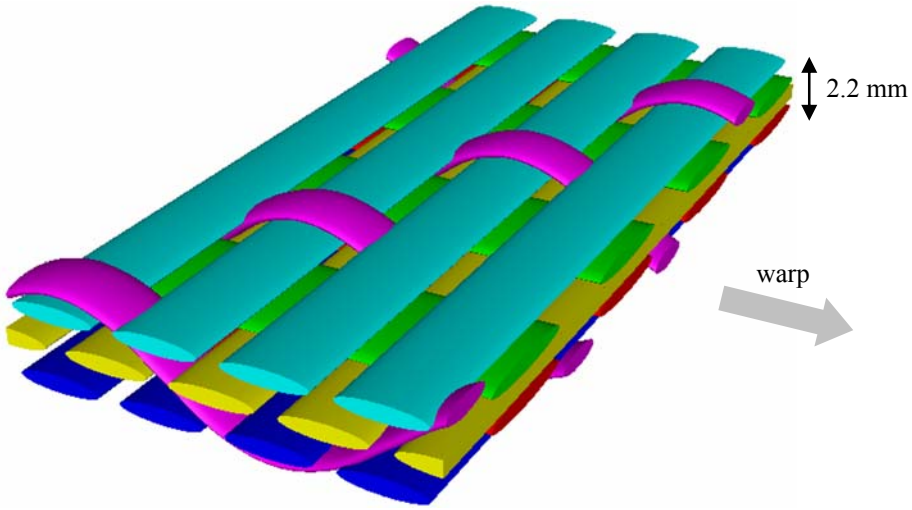

Figure 1: Idealised unit cell geometry of the through-thickness angle interlock 3D weave reinforcement, modelled in TexGen.

3. COMPRESSIBILIY

Through-thickness compression tests on circular fabric specimens with a diameter of 100 mm were carried out on a Hounsfield testing machine. The specimens were placed between two stiff plates and compressed at a relative velocity of the plates of 1 mm/min (quasi-static). The compressive force was recorded as a function of the relative displacement of the plates. The compression was stopped at a force of 10 kN (i.e. a pressure p = 12.7 bar). The absolute distance between the plates i.e. the specimen height h, was measured using a linear displacement transducer in order to calculate the fibre volume fraction at each state of compression according to

$$V_f = \frac{m}{\rho A h} \quad , \tag{1}$$

where m is the specimen mass, A is the specimen area, and $\rho = 1.75\times10^3$ kg/m^3 is the density of the carbon fibre material. The results allow the specimen thickness or fibre volume fraction to be related to a given compaction pressure.
For one dry fabric layer, the fibre volume fraction as a function of the pressure is plotted in Figure 2 for five compression cycles. The non-zero slope of the curves suggests that even at the maximum applied pressure, the fabric still shows some compliance, implying that there is still void space to be compressed. The change in fibre volume fraction under compression is significantly reduced after the first cycle, because the initial fibre packing density (i.e. initial specimen thickness) at the beginning of the second cycle is higher than for a virgin specimen. This effect is not so significant for the subsequent compression cycles.

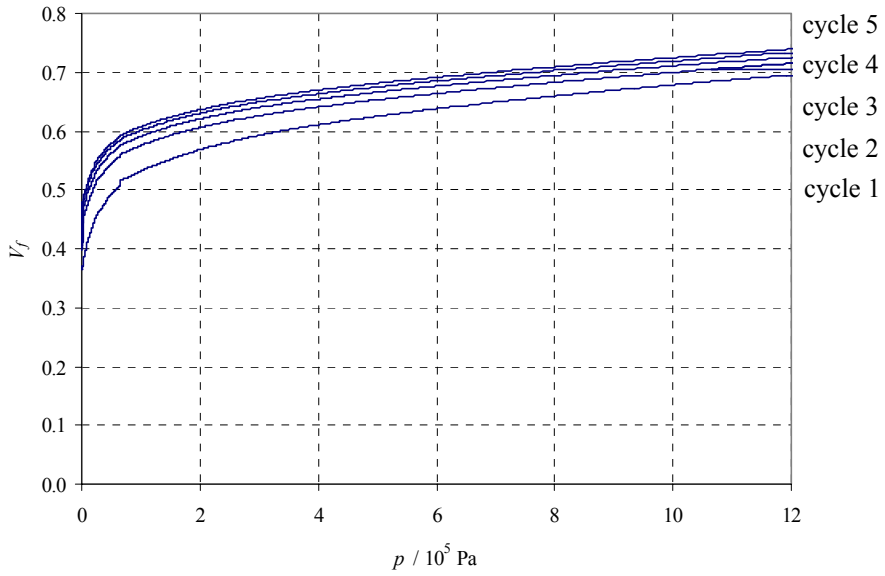

Figure 2: Fibre volume fraction V_f as a function of the compaction pressure p for five load cycles.

From the data for the compaction pressure p as a function of the specimen height h, the compressibility

$$\kappa = -\frac{1}{h_0}\frac{\Delta h}{p} \quad , \tag{2}$$

where h_0 indicates the initial specimen height at the start of the load cycle and Δh is the change in thickness during compression, can be determined. Values for the compressibility at a compaction pressure of 10 bar are listed in Table 1.

Table 1: Initial fabric height h_0, change in thickness Δh for compression at p = 10 bar, compressibility κ according to Equation (2).

cycle	1	2	3	4	5
h_0 / mm	2.25	2.06	2.02	2.00	1.99
Δh / mm	1.04	0.89	0.87	0.86	0.86
κ / 10^{-2} bar^{-1}	4.62	4.30	4.28	4.29	4.31

The values indicate that the compressibility is reduced after the first load cycle and remains approximately constant in the subsequent cycles. This suggests permanent reordering of the fibre bundles in the fabric structure during the first compression. Afterwards, the fabric behaviour in compression is mainly elastic. Compared with the values of typical 2D reinforcements, e.g. $\kappa = 3.75\times10^{-2}$ bar^{-1} for a 5-harness satin weave fabric at one layer and $\kappa = 2.84\times10^{-2}$ bar^{-1} for a UD fabric at four (aligned) layers, the compressibility is relatively high because of the large amount of void space, in particular between adjacent warp bundles (as qualitatively suggested in Figure 1).

4. GEOMETRICAL CHARACTERISATION

Geometrical characterisation of the fabric architecture is based on micrographic study at different compression levels, for which composite plaques at different thickness h and/or number of fabric layers N, were moulded. The micrographs allow the actual fibre configuration in the reinforcement structure to be determined at the micro-scale (fibre bundle level) and the meso-scale (unit cell level). The fibre bundle configuration can be related to the fabric processing properties. Its determination and quantification of the fibre bundle dimensions, allows geometry models to be generated, which show higher level of detail than that in Figure 1. These prove particularly useful in pre-processing for advanced numerical analyses, e.g. in textile micro-mechanics and simulation of textile impregnation. An example for the micrographs (one fabric layer at h = 2 mm) is shown in Figure 3. While the fibre bundle cross-sections in textile fabrics generally show characteristics of elliptical, lenticular and rectangular shapes, Figure 3 suggests that in the 3D reinforcement, the fibre bundles in the warp direction as well as the binders show almost rectangular cross-sections. The cross-sections of the bundles in the weft direction, on the other hand, tend to be more lenticular.

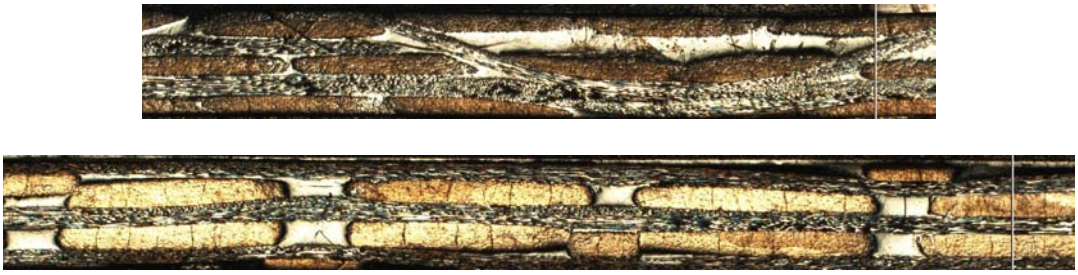

Figure 3: Micrographs of a fabric unit cell, corresponding to that in Figure 1; view along the weft direction (top) and along the warp direction (bottom) for one layer at a height of 2 mm.

From the number of fabric layers, the fabric superficial density

$$S = \frac{m}{N\,A} \quad , \tag{3}$$

the plaque thickness and the density of the carbon fibre material, the fibre volume fraction for each moulded specimen was determined according to Equation (1). The corresponding compaction pressure can then be determined from the curve for the first load cycle in Figure 2. Micrographs were taken for one fabric layer at a plaque thickness h = 2 mm (corresponding to V_f = 0.41, p = 0.09×10^5 Pa), two layers at h = 3.5 mm (V_f = 0.47, p = 0.34×10^5 Pa) and three layers at h = 4.6 mm (V_f = 0.54, p = 1.20×10^5 Pa). The measured dimensions of the fibre bundles and the inter-bundle voids are listed in Table 2.

Table 2: Dimensions of fibre bundles and inter-bundle voids (mean values, standard deviations and coefficients of variation), determined from digital analysis of micrographs at different compression levels.

	fibre bundles		inter-bundle voids	
	width / mm	height / mm	width / mm	height / mm
	N = 1, h = 2 mm, V_f = 0.41, p = 0.09×10^5 Pa			
warp	4.01 ± 0.19 (± 5 %)	0.41 ± 0.03 (± 7 %)	0.97 ± 0.12 (± 13 %)	0.31 ± 0.06 (± 21 %)
weft	3.16 ± 0.19 (± 6 %)	0.38 ± 0.04 (± 10 %)	0.49 ± 0.20 (± 40 %)	0.34 ± 0.04 (± 11 %)
binder	1.40 ± 0.16 (± 11 %)	0.37 ± 0.07 (± 19 %)	-	-
	N = 2, h = 3.5 mm, V_f = 0.47, p = 0.34×10^5 Pa			
warp	4.02 ± 0.21 (± 5 %)	0.42 ± 0.05 (± 12 %)	0.83 ± 0.15 (± 18 %)	0.23 ± 0.05 (± 20 %)
weft	3.29 ± 0.20 (± 6 %)	0.45 ± 0.07 (± 15 %)	0.42 ± 0.20 (± 47 %)	0.30 ± 0.05 (± 17 %)
binder	1.48 ± 0.16 (± 11 %)	0.35 ± 0.04 (± 11 %)	-	-
	N = 3, h = 4.6 mm, V_f = 0.54, p = 1.20×10^5 Pa			
warp	4.66 ± 0.25 (± 5 %)	0.39 ± 0.05 (± 12 %)	0.86 ± 0.32 (± 37 %)	0.23 ± 0.06 (± 25 %)
weft	3.30 ± 0.23 (± 7 %)	0.23 ± 0.04 (± 20 %)	0.35 ± 0.13 (± 36 %)	0.21 ± 0.03 (± 12 %)
binder	1.19 ± 0.34 (± 29 %)	0.26 ± 0.03 (± 12 %)	-	-

A general observation is that for N = 2 and N = 3, the measured thickness values in Table 2 do not necessarily add up to the total specimen thickness. Due to the effect of nesting between adjacent fabric layers, the sum of the apparent layer thicknesses may be greater than the specimen thickness. Because of local lateral compression caused by the warp bundles, the width of the binder varies more strongly than that of the weft and warp bundles. While the fabric thickness decreases in compression, the length of the binder remains constant. This results in a change of curvature of the binder, which may cause local variations in the fabric structure.

Comparison of the dimensions for one layer at h = 2 mm and two layers at h = 3.5 mm suggests that, at low levels of fabric compression, the layer height is reduced mainly by local reduction of the height of voids between the bundles in the warp direction rather than by bundle compression and change of the bundle cross-section. In fabric compression, the binder tows on the fabric surface are pushed into the voids, locally

bending the weft bundles and pushing the warp bundles apart (Figure 4, bottom). The variation of the width of the voids between adjacent weft bundles is significantly higher than that of the voids between adjacent warp bundles. This is caused by the presence of the binder, which locally pushes the weft bundles apart or together (Figure 4, top).
Comparison of the dimensions for two layers at h = 3.5 mm and three layers at h = 4.6 mm suggests that, at higher levels of compression, the layer height is reduced by bundle compression and (local) change of the bundle cross-section. This is reflected in a trend for the width of the warp bundles to increase and the height of the weft bundles to decrease. Since the height of the warp bundles and the width of the weft bundles does not change significantly, and reduction of the total bundle volume (or cross-sectional area) by compression of inter-filament voids is limited, this implies that the cross-section of the warp bundles becomes more elliptical (or lenticular), and that of the weft bundles more rectangular. For the binder, both width and height tend to decrease, suggesting that the bundles become more rectangular. The absolute dimensions of the inter-bundle voids remain constant in the warp direction and tend to be slightly reduced in the weft direction.
Due to increased local lateral compression, the variation in binder width increases significantly. This is correlated to a significant increase in variation of the width of the voids in the warp direction caused by the effect schematically illustrated in Figure 4 (bottom). The height of the weft bundles shows increased variation because of local compression by the binder (Figure 4, top).

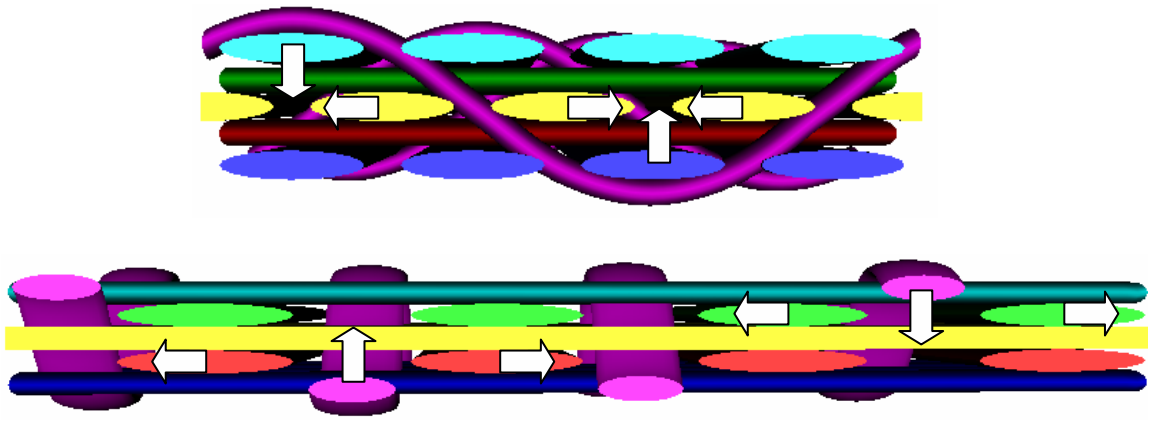

Figure 4: Schematic illustration of main deformation mechanisms of a fabric unit cell in compression; view along the weft direction (top) and along the warp direction (bottom); arrows indicate bundle movement during reordering.

5. PERMEABILITY

The unsaturated in-plane permeability of the 3D woven fabric was measured in radial injection experiments at constant injection pressure. The experimental set-up and procedure is described in detail elsewhere [5]. The results for the principal in-plane permeability values K_1 and K_2, the ratio K_1/K_2, characterising the anisotropy of the permeability, and the angle θ between the fabric weft direction and the principal flow direction, are listed in Table 3 at different fibre volume fractions V_f.

Table 3: Principal in-plane permeability values K_1 and K_2, ratio of anisotropy K_1/K_2 and angle θ between the fabric weft direction and the principal flow direction, as functions of the fibre volume fraction V_f (mean values, standard deviations and coefficients of variation are given where applicable); number of layers N and cavity height h are also given.

V_f	N	h / mm	K_1 / 10^{-10} m^2	K_2 / 10^{-10} m^2	K_1/K_2	θ
0.41 ± 0.00	1	2	17.403 ± 6.237 (± 36 %)	6.067 ± 2.178 (± 36 %)	3.108 ± 1.554 (± 50 %)	-29° ± 4°
0.47 ± 0.00	2	3.5	9.999 ± 5.331 (± 53 %)	1.913 ± 0.471 (± 25 %)	5.201 ± 2.676 (± 51 %)	-26° ± 6°
0.50 ± 0.00	3	5	1.599 ± 0.563 (± 35 %)	0.697 ± 0.056 (± 8 %)	2.343 ± 0.982 (± 42 %)	-24° ± 5°
0.55 ± 0.01	2	3	0.510 ± 0.149 (± 29 %)	0.343 ± 0.052 (± 15 %)	1.463 ± 0.218 (± 15 %)	-30° ± 11°
0.62 ± 0.00	3	4	0.169 ± 0.054 (± 32 %)	0.134 ± 0.026 (± 20 %)	1.240 ± 0.169 (± 14 %)	-24° ± 17°

Table 4: Principal in-plane permeability values K_1 and K_2, ratio of anisotropy K_1/K_2 and angle θ between the fabric weft direction and the principal flow direction, as functions of the fibre volume fraction V_f (mean values, standard deviations and coefficients of variation are given where applicable); these data refer to examples of 2D fabrics (for comparison).

V_f	K_1 / 10^{-10} m^2	K_2 / 10^{-10} m^2	K_1/K_2	θ
		UD fabric		
0.49 ± 0.00	6.334 ± 0.525 (± 8 %)	1.140 ± 0.155 (± 14 %)	5.60 ± 0.57 (± 10 %)	84° ± 5°
0.58 ± 0.00	1.395 ± 0.304 (± 22 %)	0.165 ± 0.033 (± 20 %)	8.77 ± 2.64 (± 30 %)	86° ± 3°
0.68 ± 0.01	0.386 ± 0.138 (± 36 %)	0.067 ± 0.037 (± 55 %)	6.37 ± 2.22 (± 35 %)	86° ± 6°
		5-hs satin weave fabric		
0.43 ± 0.00	1.665 ± 0.178 (± 11 %)	1.274 ± 0.106 (± 8 %)	1.32 ± 0.23 (± 17 %)	109° ± 12°
0.52 ± 0.00	0.557 ± 0.007 (± 1 %)	0.457 ± 0.027 (± 6 %)	1.22 ± 0.07 (± 6 %)	90° ± 9°
0.61 ± 0.00	0.472 ± 0.047 (± 10 %)	0.208 ± 0.019 (± 9 %)	2.28 ± 0.21 (± 9 %)	91° ± 1°
0.70 ± 0.01	0.194 ± 0.015 (± 8 %)	0.129 ± 0.003 (± 2 %)	1.50 ± 0.09 (± 6 %)	89° ± 2°

Both in-plane principal permeability values are generally in the order of 10^{-10} m^2 and, as expected, decrease strongly with increasing fibre volume fraction. The orientation of the principal permeability axes reflects the angle between the fabric weft direction and the through-thickness pattern of the binder tows as visible on the surfaces of a fabric layer (see Figure 1). It is independent of the fibre volume fraction. This indicates that the inter-bundle voids created by the binder dominate the fabric permeability.
For comparison, in-plane permeability data for the 5-harness satin weave fabric and the UD fabric are listed in Table 4. The permeability values of all fabrics are in the same order of magnitude for similar ranges of V_f. However, for the 3D fabric, the change in permeability with increasing V_f is generally more significant than for the other fabrics. This is caused by the significant reduction of the inter-bundle void volume discussed above, and related to the higher compressibility.
The through-thickness permeability K_3 was measured in saturated flow experiments at constant flow rate, as described e.g. by Goulley et al. [6]. The results for K_3 are listed in Table 5 at different fibre volume fractions V_f. Compared with the through-thickness permeability of the satin weave fabric, for which $K_3 = (1.335 \pm 0.299) \times 10^{-12}$ m^2 at $V_f = 0.64$, the measured values are relatively high. The difference is caused by the presence of the binder, which creates flow-enhancing through-thickness channels in the structure of the 3D reinforcement.

Table 5: Through-thickness permeability K_3 as a function of the fibre volume fraction V_f (mean values, standard deviations and coefficients of variation are given where applicable); number of layers N and cavity height h are also given.

V_f	N	h / mm	K_3 / 10^{-12} m^2
0.40 ± 0.00	2	4	23.512 ± 7.498 (± 32 %)
0.50 ± 0.00	3	5	14.266 ± 3.150 (± 22 %)
0.63 ± 0.00	3	4	8.699 ± 3.087 (± 36 %)

6. CONCLUSIONS

For a carbon fibre 3D reinforcement with through-thickness angle interlock weave architecture, the compressibility, geometrical structure at different compression levels and permeability at different fibre volume fractions was studied experimentally. Compressibility and permeability were related to the textile architecture and compared with the properties of examples for 2D reinforcements.
The compression behaviour was studied in five load cycles. Due to permanent reordering of the fibre bundles in the fabric structure, the compressibility is reduced after the first cycle. In the subsequent compression cycles, the fabric behaviour is mainly elastic, and the compressibility remains approximately constant. Compared with typical 2D reinforcements, the compressibility is relatively high.
Microscopic study of the fabric structure suggests that this is caused by the large amount of void space in the 3D fabric, in particular between adjacent warp bundles. At low levels of fabric compression, the layer height is reduced mainly by local reduction of the height of voids between the bundles in the warp direction rather than by bundle compression and change of the bundle cross-section. The binder tows on the fabric surface are pushed into the voids, locally bending the weft bundles and pushing the warp bundles apart. At higher levels of compression, the layer height is reduced by bundle compression and change of the bundle cross-section. Due to increased local

lateral compression, significantly increased variation in binder width is correlated to a significant increase in variation of the width of the voids in the warp direction.
Both in-plane principal permeability values are generally in the same order of magnitude as those of 2D fabrics. Because of the significant reduction of the inter-bundle void volume, which is related to the higher compressibility, the decrease in permeability with increasing fibre volume fraction is more significant than for 2D fabrics. The orientation of the principal permeability axes reflects the angle between the fabric weft direction and the pattern of the binder tows. It is independent of the fibre volume fraction. The inter-bundle voids created by the binder dominate the fabric permeability. The through-thickness permeability is higher than that of a typical 2D fabric. Flow-enhancing through-thickness channels in the structure of the 3D reinforcement are formed around the binder tows.

ACKNOWLEDGEMENTS
This work was funded by the Engineering and Physical Science Research Council (EPSRC), as part of Platform Grant GR/T18578/01, and the Nottingham Innovative Manufacturing Research Centre. The authors wish to thank Carr Reinforcements Ltd. for supply of woven fabrics.

REFERENCES

1- Potluri, P., Sharma, S., Ramgulam, R., "Comprehensive drape modelling for moulding 3D textile preforms", *Composites Part A*, 2001; 32: 1415-1424.
2- Desplentere, F., Lomov, S., Woerdeman, D., Verpoest, I., Wevers, M., Bogdanovich, A., "Micro-CT characterization of variability in 3D textile architecture", *Composites Part A*, 2005; 65: 1920-1930.
3- Adanur, S., Liao, T., "3D modeling of textile composite preforms", *Composites Part B*, 1998; 29: 787-793.
4- TexGen (Version 3.2.1), University of Nottingham, 2007: http://texgen.sourceforge.net (viewed 10.03.2008).
5- Endruweit, A., McGregor, P., Long, A.C., Johnson, M.S., "Influence of the fabric architecture on the variations in experimentally determined in-plane permeability values", *Composites Science and Technology*, 2006; 66: 1778-1792.
6- Goulley, G., Pitard, P., Pabiot, J., "Longitudinal and Transversal Permeability Measurement of Glass Fiber Reinforcement for the Modelling of Flow in RTM", *Proceedings of the 6th European Conference on Composite Materials*, Bordeaux, 1993: 83-88.